Supporting Information for

Integrated photoelectrochemical energy storage: solar hydrogen generation and supercapacitor

Xinhui Xia[1,3,‡], Jingshan Luo[1,‡], Zhiyuan Zeng[2], Cao Guan[1], Yongqi Zhang[3], Jiangping Tu[3], , Hua Zhang[2] & Hong Jin Fan[1*]

[1] Division of Physics and Applied Physics, School of Physical and Mathematical Sciences, Nanyang Technological University, Singapore 637371, Singapore

[2]School of Materials Science and Engineering, Nanyang Technological University, Singapore 639798, Singapore

[3] State Key Laboratory of Silicon Materials and Department of Materials Science and Engineering, Zhejiang University, Hangzhou 310027, P. R. China

[*] Corresponding author. Email: fanhj@ntu.edu.sg

[‡] These authors contributed equally to this work

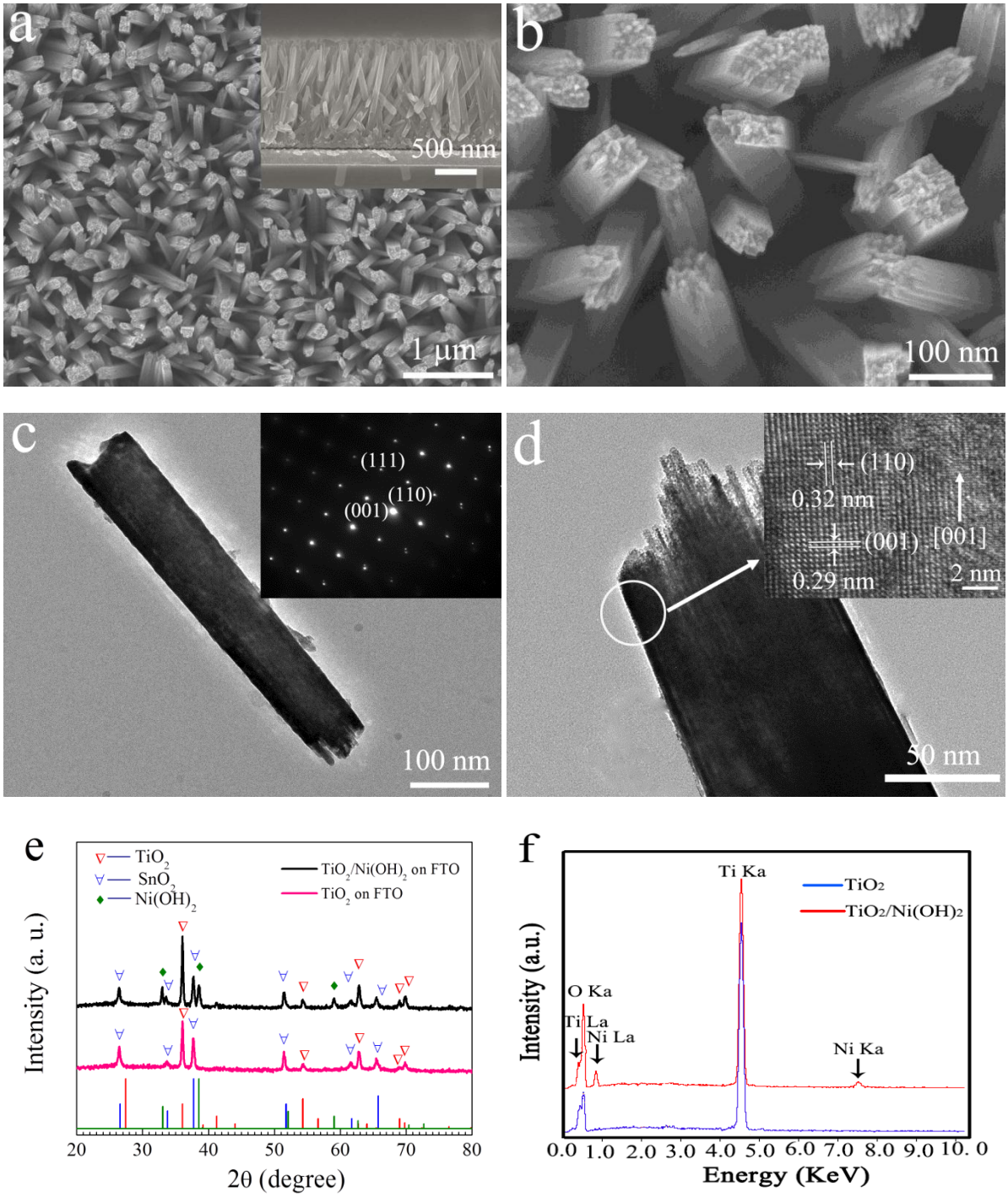

Figure S1. Characterization of the TiO_2 nanorods. (a) SEM image of the nanorod array. The side view is provided in inset. (b) Enlarged top-view of the nanorod array. (c and d) TEM images of individual TiO_2 nanorod with the corresponding electron diffraction pattern and HRTEM image, respectively. (e) XRD pattern of the TiO_2 nanorod array and the $TiO_2/Ni(OH)_2$ core/branch nanorod array. (f) EDS spectra of the pure TiO_2 nanorod and $TiO_2/Ni(OH)_2$ core/branch nanorods.

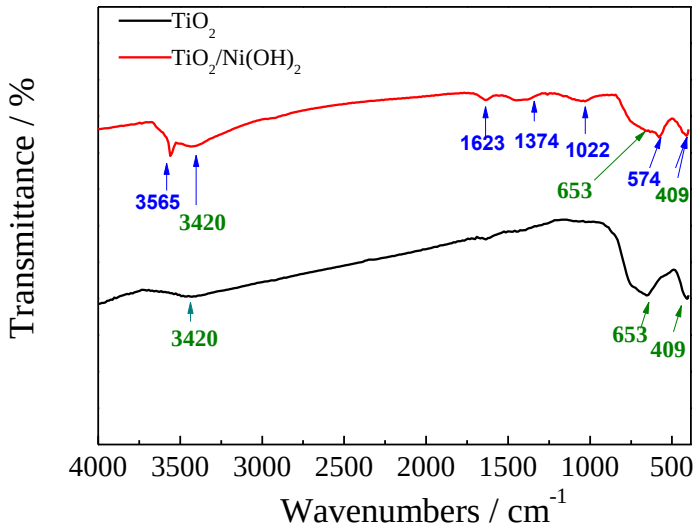

Figure S2. FTIR spectra of TiO_2 and $TiO_2/Ni(OH)_2$ core/shell nanorods scratched from FTO substrates.

In the FTIR spectrum of the $TiO_2/Ni(OH)_2$ core/shell nanorod, the peak around 3565 cm^{-1} is characteristic of non-hydrogen bonds O-H stretching vibrations of β-$Ni(OH)_2$. A broad OH band centered 3420 cm^{-1} is indicative of hydrogen bonded water within the film structure and the band at 1623 cm^{-1} corresponds to the angular deformation of molecular water. The peaks in the range of 1022-1374 cm^{-1} belong to SO_4^{2-} from the reagents. The bands at 574 cm^{-1} correspond to δ(OH) vibration. Both samples have peaks centered at 653 and 409 cm^{-1} characteristic of rutile TiO_2.

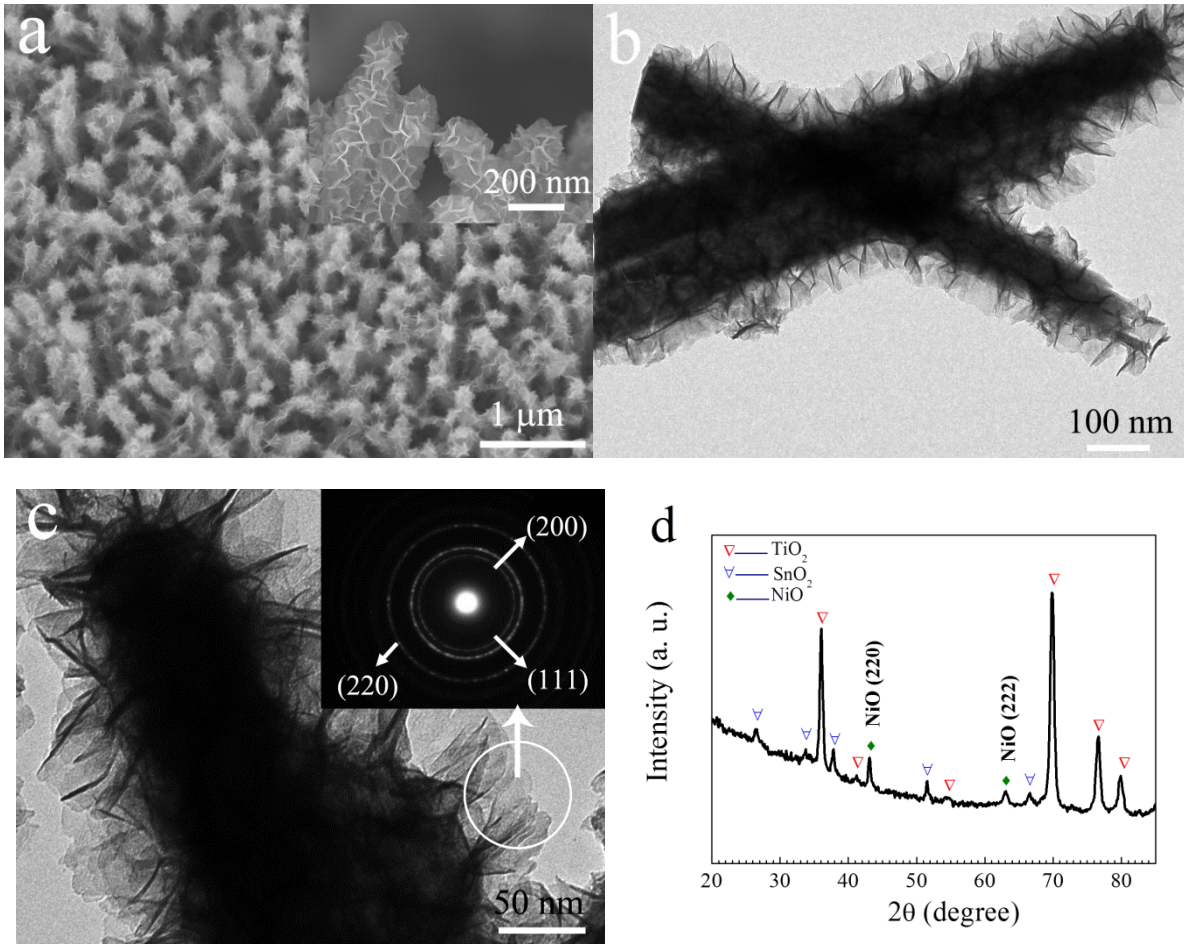

Figure S3. TiO_2/NiO core/shell nanorod arrays**. (a)** SEM image of TiO_2/NiO core/shell nanorod arrays. **(b), (c)** TEM images of TiO_2/NiO core/shell nanorods (SAED pattern in inset). The nanoflake shell has a polycrystalline SAED pattern corresponding to cubic NiO phase. **(d)** XRD pattern of TiO_2/NiO core/shell nanorod arrays on FTO, showing that the core/shell nanorod arrays contain rutile TiO_2 (JCPDS 88-1175) and cubic NiO phase (JCPDS 4-0835).

Synthesis of self-supported $TiO_2/Co(OH)_2$ core/shell nanorod arrays

$TiO_2/Co(OH)_2$ core/shell nanorod arrays were prepared by the combination of hydrothermal synthesis and cathodic electrodeposition methods. The TiO_2 nanorod arrays on FTO were first grown via the hydrothermal synthesis method as mentioned above. Then the TiO_2 nanorod arrays were used as the scaffold for $Co(OH)_2$ nanoflake growth through a facile electrodeposition method. Electrolyte for electrodeposition was obtained by dissolving 6 g $Co(NO_3)_2$ and 0.85 g $NaNO_3$ into 100 ml distilled H_2O. The electrodeposition of $Co(OH)_2$ was carried out in a three-compartment system, the above TiO_2 nanorod arrays electrode as the working electrode, Ag/AgCl electrode as the reference electrode and a Pt foil as the counter-electrode. The $Co(OH)_2$ was deposited by cyclic voltammetry as follows: two cycles were conducted in the potential range of -0.4 – -1 V with a sweep rate of 10 mV s^{-1}. Finally, the samples were taken off and rinsed with distilled water. The load weight of the $Co(OH)_2$ is approximately 0.16 mg cm^{-2}. The SEM images of the obtained core/shell nanorod arrays and XRD pattern are shown in Fig. S4.

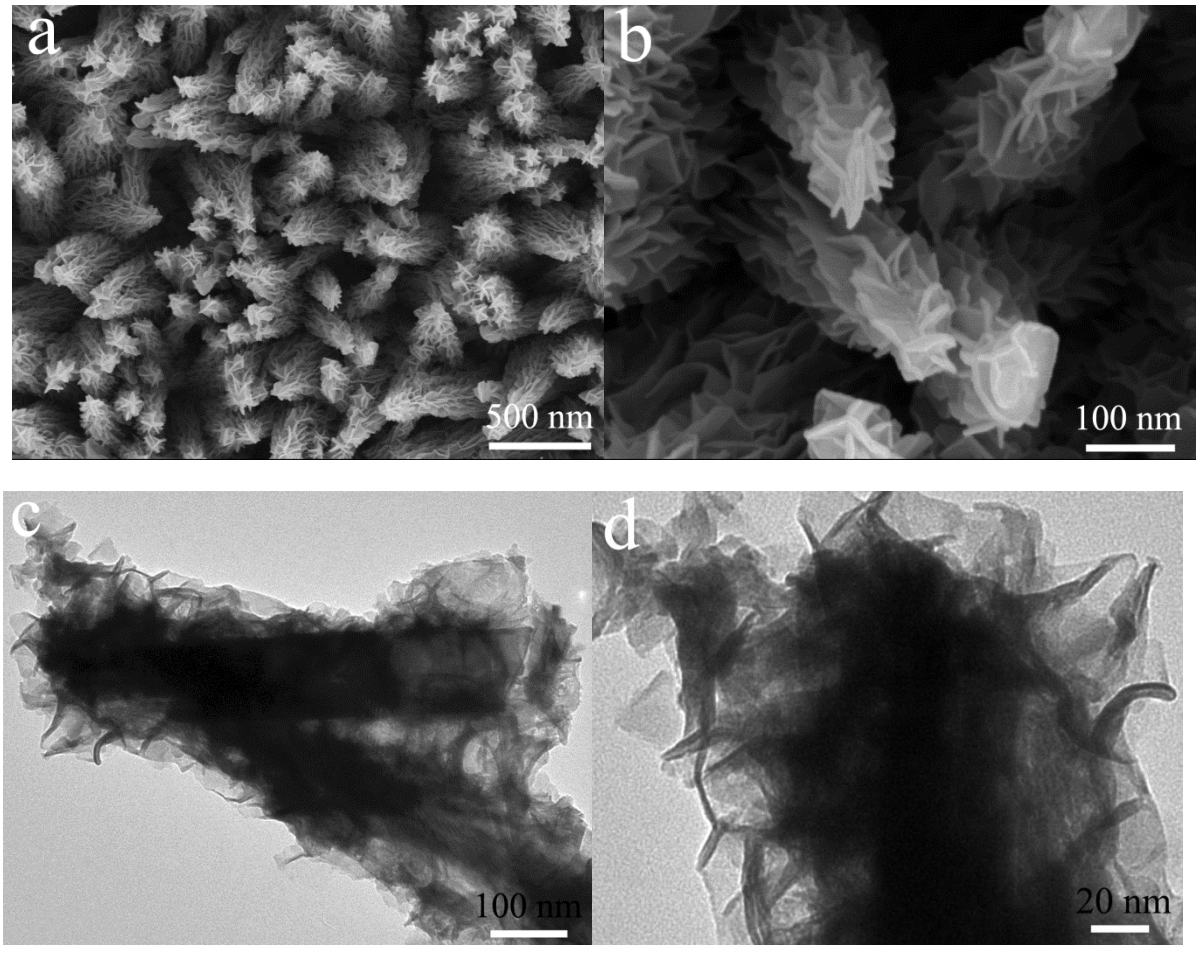

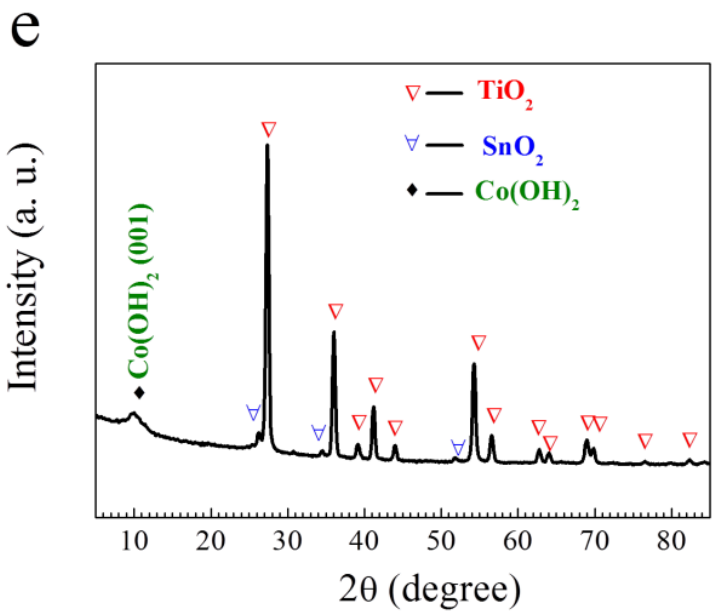

Figure S4. $TiO_2/Co(OH)_2$ core/shell nanorod arrays. **(a), (b)** SEM images of $TiO_2/Co(OH)_2$ core/shell nanorod arrays prepared by the combination of hydrothermal synthesis and cathodic electrodeposition. **(c), (d)** TEM images of $TiO_2/Co(OH)_2$ core/shell nanorods. The $Co(OH)_2$ nanoflakes have a thickness around 10 nm. **(e)** XRD pattern of $TiO_2/Co(OH)_2$ core/shell nanorod arrays on FTO. The electrodeposited $Co(OH)_2$ is indexed to the α-$Co(OH)_2$ phase (JCPDS 74-1057).

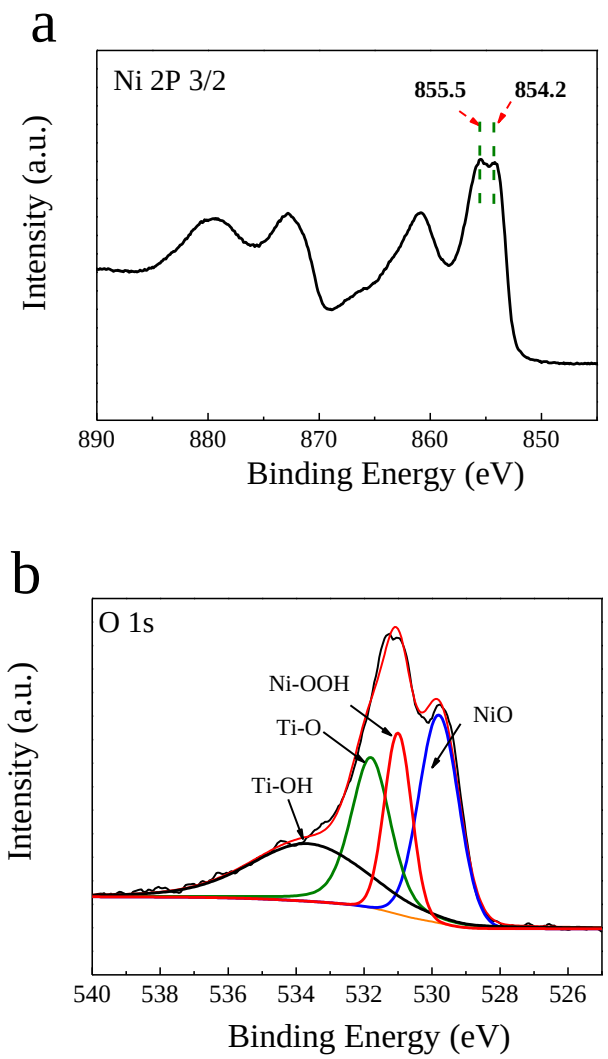

Figure S5. XPS spectra of $TiO_2/Ni(OH)_2$ core/shell nanorod arrays after photooxidation (a) Ni $2p_{3/2}$ and (b) O 1s.

Notice that Ni $2p_{3/2}$ peak has two separated components. The peak at 854.2 eV is due to Ni–O bonds and the other one at 855.5 eV corresponds to Ni-OOH bonds. The Ni-OOH bonds mainly come from higher valence nickel hydroxides (NiOOH) or $4Ni(OH)_2 \cdot NiOOH \cdot xH_2O$. In the O1s spectra, the peak at 531.3 eV indicates the existence of Ni-OOH bonds, which is also consistent with the Ni $2p_{3/2}$ spectrum. The key results from the XPS test indicate that $Ni(OH)_2$ can be photooxidized by the holes.

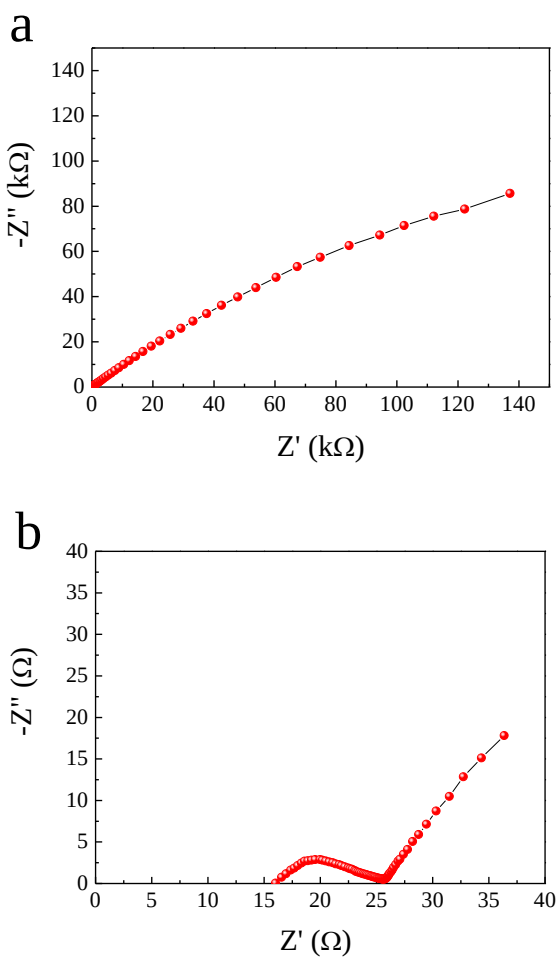

Figure S6. Nyquist plots of $TiO_2/Ni(OH)_2$ core/shell nanorod arrays (a) before and (b) after discharge.

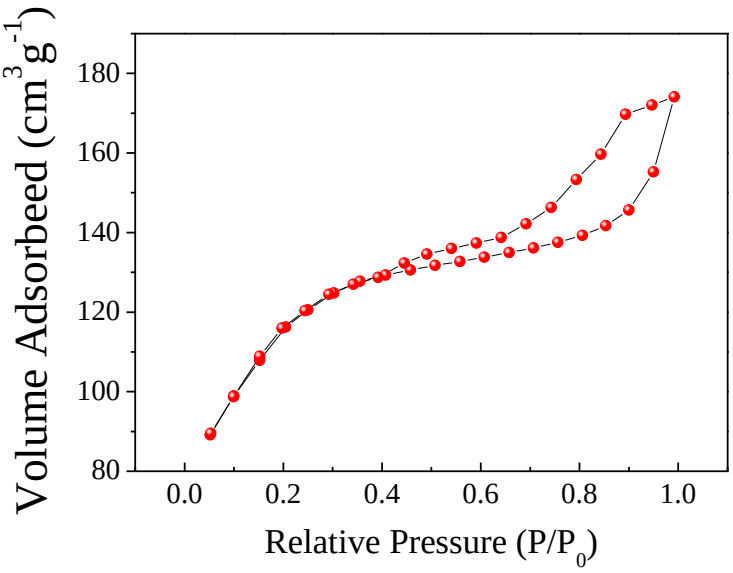

Figure S7. BET measurement of $TiO_2/Ni(OH)_2$ core/shell nanorod arrays. The measured surface area is about 198 m^2 g^{-1}.

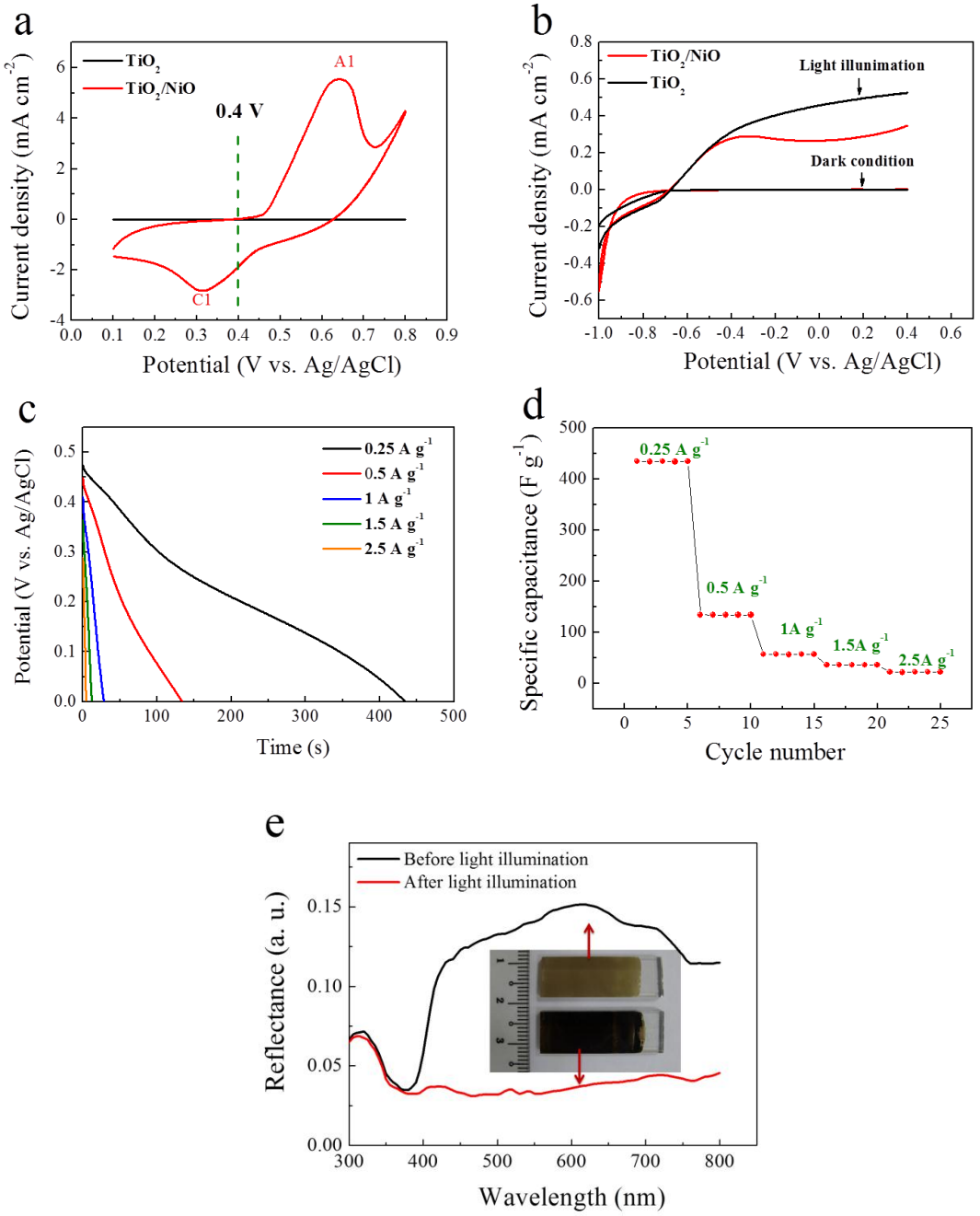

Figure S8. Photoelectrochemical and pseudocapacitive characterizations of TiO_2/NiO core/shell nanorod arrays. **(a)** CV curves of TiO_2 and TiO_2/NiO core/shell nanorod arrays on FTO in the potential region of 0.1– 0.8 V at a scanning rate of 10 mV s^{-1} at the second cycle**. (b)** *J*−V curves under dark condition and simulated solar light illumination. **(c)** Discharge curves of the core/shell nanorod arrays with simulated solar light illumination at 0.4 V bias for 300 s at various discharge current densities. **(d)** Specific capacitances of the core/shell nanorod arrays at various discharge current densities. **(e)** Diffuse reflectance spectra of the core/shell nanorod arrays before and after discharge (Inset: photographs of samples).

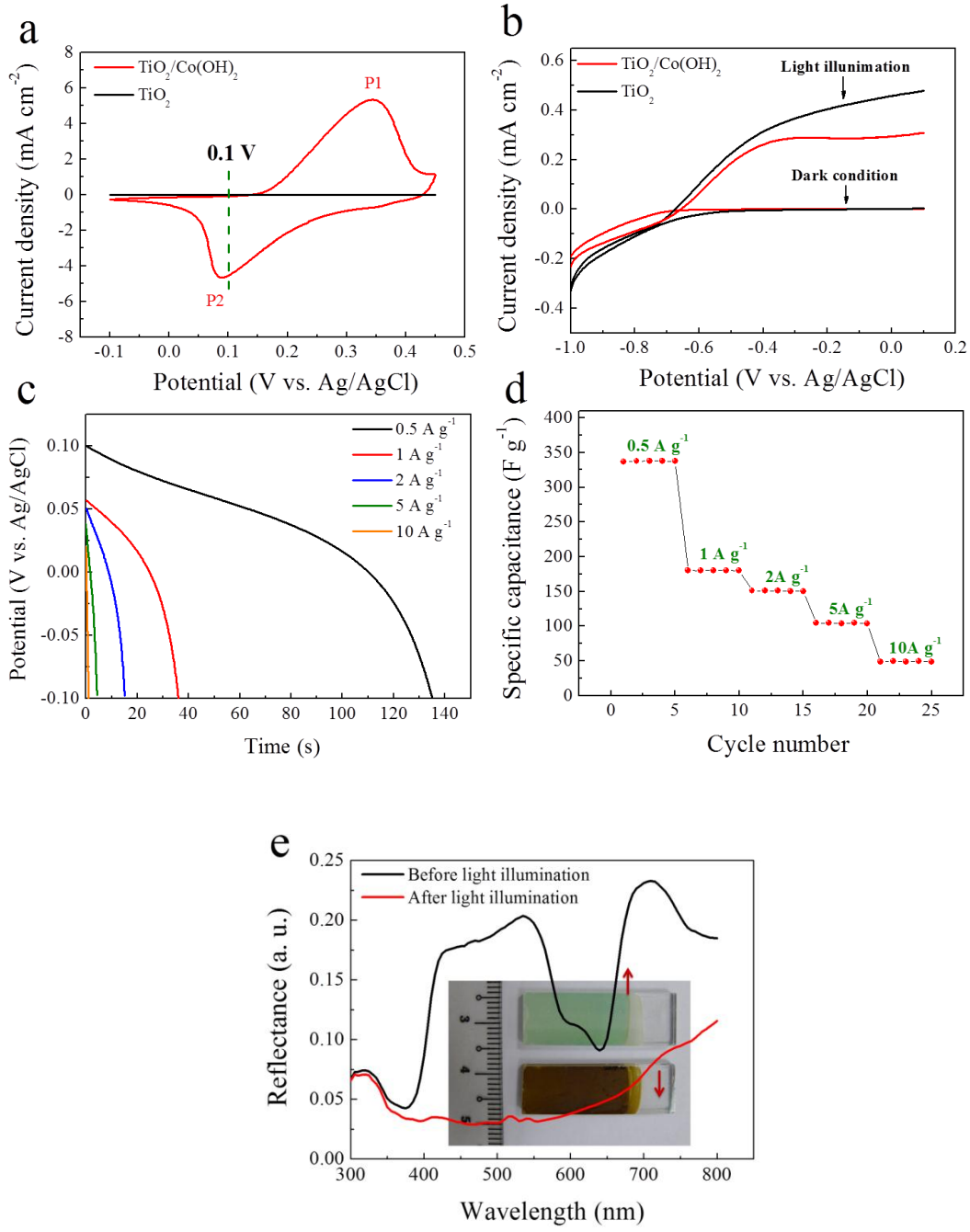

Figure S9. Photoelectrochemical and pseudocapacitive characterizations of TiO_2/$Co(OH)_2$ core/shell nanorod arrays. (a) CV curves of TiO_2 and the TiO_2/$Co(OH)_2$ core/shell nanorod arrays on FTO in the potential region of -0.1– 0.45 V at a scanning rate of 10 mV s^{-1} at the second cycle**. (b)** *J*–V curves under dark condition and simulated solar light illumination. **(c)** Discharge curves of the core/shell nanorod arrays with simulated solar light illumination at 0.1 V bias for 300 s at various discharge current densities. **(d)** Specific capacitances of the core/shell nanorod arrays at various discharge current densities. **(e)** Diffuse reflectance spectra of the core/shell nanorod arrays before and after discharge (Inset: photographs of samples).